Iterative Detection using MMSE-PIC Demapping for MIMO-GFDM Systems

Maximilian Matthé, Dan Zhang, Gerhard Fettweis

Vodafone Chair Mobile Communication Systems, Technische Universität Dresden, Germany
{maximilian.matthe,dan.zhang,fettweis}@ifn.et.tu-dresden.de

***Abstract*—Diverse requirements are foreseen for the 5G cellular system and new waveforms are being researched for the physical layer (PHY), where the non-orthogonal Generalized Frequency Division Multiplexing (GFDM) is one candidate. Its inherent self-interference makes receiver design challenging, particularly when besides inter-carrier interference (ICI) and inter-symbol interference (ISI) also inter-antenna interference (IAI) occurs, as in systems that employ spatial multiplexing (SM) to increase the throughput. To encounter this interference, we apply the prominent minimum mean squared error with parallel interference cancellation (MMSE-PIC) iterative receiver structure to GFDM, and provide a formulation that is suitable for a low-complexity implementation. We analyze the decoding performance employing a well-known current WiMax LDPC code. The proposed demapping algorithm can be implemented with complexity that scales linearly with the number of subcarriers of the system. Analysis of information transfer characteristics shows that the MMSE-PIC demapper for GFDM exhibits potential to outperform the OFDM demapper with a matching code, however, simulations of frame error rate (FER) show inferior performance of GFDM. These results emphasize the importance of a joint waveform and code design in order to exploit the full potential of the MMSE-PIC receiver structure for GFDM.**[1]

I. Introduction

The upcoming fifth generation (5G) of cellular mobile networks will pose diverse requirements on the underlying physical layer (PHY) of the system. As such, not only a massively increased data rate but also improved flexibility, coexistence and significantly reduced latency are demanding challenges [1]. Even though not all criteria are required to be fulfilled for a single use case, it is desirable that a single flexible PHY is able to fulfill these demands simply by changing configuration options [2]. Among other waveforms such as universally filtered OFDM [3] and Filterbank multicarrier (FBMC) [4], Generalized Frequency Division Multiplexing (GFDM) [5] has been proposed as a 5G candidate waveform, that matches well the foreseen requirements. Its good spectral localization makes it suitable for coexisting asynchronous systems [6]; whereas its circular structure aids block-processing in the frequency domain, giving rise for low-complexity implementations of transmitter and linear receivers [7].

Key methods for increasing the data rate of a system include widening the transmit band width or increasing the number of transmit and receive antennes. Widening the transmit band width is commonly achieved by either carrier aggregation [8] or moving to the mmWave frequency band [9], where wide continuous frequency bands are available.

Applying multiple-input multiple-output (MIMO) techniques to increase the overall system's data rate has been thoroughly researched during the last 50 years [10] and different MIMO techniques will be applied to any 5G system. Thus, any 5G waveform candidate is required to be compatible with different MIMO techniques. The implementation complexity increases significantly with the system size, and hence low-complexity solutions are significantly important, especially with upcoming Massive MIMO techniques [11].

The equivalent channel of a GFDM system can be understood as a large-scale MIMO system and hence common MIMO techniques can be applied. GFDM was presented to be compatible with both the Alamouti Space-Time coding technique [12], [13] and with spatial multiplexing (SM) [14], [15], [16]. In [16] linear receiver techniques for GFDM have been shown to obtain poor coded performance compared to orthogonal schemes as Orthogonal Frequency Division Multiplexing (OFDM). However, in [15] a non-linear receiver technique is presented that combines a sphere decoder (SD) with successive interference cancellation (SIC) to achieve significant gains in the uncoded case compared to an equivalent OFDM system.

Furthermore, in [17] it was suggested, that in principle GFDM can achieve a higher coded capacity than OFDM, when the fading channel becomes severely frequency selective, as it can appear in low latency scenarios, employing short packets [1]. Additionally, in [14] a non-linear iterative receiver structure was presented, that can actually achieve higher throughput than an equivalent OFDM system.

In this paper, we tailor the well understood minimum mean squared error with parallel interference cancellation (MMSE-PIC) iterative detection scheme [18], [19], [20] for MIMO detection of spatially multiplexed GFDM streams. In particular, we exploit the specific system structure of GFDM to yield an algorithm with reduced complexity compared to common approaches, e.g. from [20]. MMSE-PIC has been successfully applied to OFDM transmission schemes [21] and shown to perform close to the optimal maximum likelihood (ML) detection which is achieved with a high-complexity SD. Since each iteration in MMSE-PIC is merely a linear detection, the overall system complexity is far below that of an optimal SD approach, especially when the system size increases.

[1]Rudimentary MATLAB code can be acquired from http://wwwpub.zih.tu-dresden.de/~vf5gdemo/GFDM/.

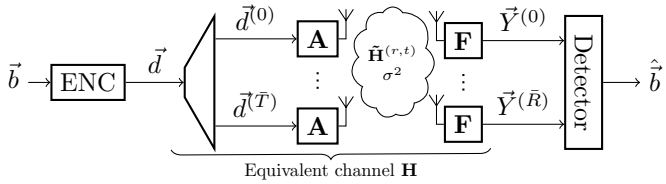

Fig. 1. Block diagram of the MIMO-GFDM system.

Subsequently, we will derive the equivalent MIMO system model for GFDM, from which we shortly present the MMSE-PIC iteration process. Because of inherent inter-carrier interference (ICI) and inter-symbol interference (ISI), the equivalent system matrix is significantly larger than that of an equivalent OFDM system. Accordingly, applying conventional linear detection to this problem might already be too complex on todays hardware. Hence, we reformulate the detection equations, leading to an algorithm which reduces the computational burden of each iteration. We exploit the band-diagonal structure of the resulting system matrix to yield an implementation concept which scales linearly with the number of subcarriers. Additionally, we employ an algorithm proposed in [22] that is used to estimate the diagonal of an inverse matrix without explicitely calculating this inverse. This technique efficiently reduces implementation complexity further. We show that, depending on the rolloff of the pulse shaping filter for GFDM and channel characteristics, the same frame error rate (FER) as for OFDM can be achieved with the non-orthogonal GFDM system. However, for longer channels the analyzed system yields inferior performance. Subsequent analysis of the information transfer characteristices of the GFDM and OFDM MMSE-PIC demapping process reveals a superior potential for GFDM.

The remainder of this paper is organized as follows: Sec. II introduces the GFDM system and derives the overall system model. This system model is used in Sec. III for the derivation of the MMSE-PIC demapping process and also the low-complexity formulation of the process is provided. Sec. IV presents simulation results, comparing OFDM and GFDM MMSE-PIC coded performance in various channel conditions and provides analysis of the information transfer characteristic of both systems. Finally, conclusions are drawn in Sec. V.

Notation: $\vec{x}$, $\mathbf{X}$, $\mathbf{X}^{\mathrm{T}}$, $\mathbf{X}^{\mathrm{H}}$, $\circ$ and $\oslash$ denote vectors, matrices, transpose, conjugate transpose, and elementwise multiplication and division, respectively. $\Lambda = \mathrm{diag}(x_1, \ldots, x_N)$ is a diagonal matrix with $\Lambda_{ii} = x_i$ and $\mathrm{diag}(\mathbf{X})$ is the diagonal of $\mathbf{X}$ as a vector. $\vec{1}$ is a column vector of all ones. $\lceil x \rceil_2$ denotes the smallest power-of-two that is greater or equal to x. $\mathrm{DFT}_N\{\cdot\}$ and $\mathbf{F}$ denote N-point discrete Fourier transform (DFT) and DFT matrix. Finally, $\langle x \rangle_N$ is the remainder of x modulo N.

II. System Model

A. Transceiver Model

Consider a $R \times T$ MIMO system with R receive and T transmit antennas. The system operates in SM mode with no channel state information (CSI) at the transmitter, as illustrated in Fig. 1, where $\bar{T} = T - 1, \bar{R} = R - 1$. The payload bit vector $\vec{b}$ is encoded and mapped to complex constellation symbols with a channel coder in the *ENC* block. Then, the data is split into independent streams and one GFDM block is transmitted from each antenna with equally distributed power.

Each GFDM block consists of $N = KM$ samples and is divided into K subcarriers and M subsymbols. The data symbol transmitted on the kth subcarrier in the mth transmit symbol from the tth transmit antenna is denoted by $d_{k,m}^{(t)}$ and taken from a complex quadrature amplitude modulation (QAM) constellation set $\mathcal{S}$. The data symbols are transmitted on circularly time-frequency shifted versions of the prototype filter $g[n]$, which are critically sampled in the time-frequency plane, i.e. $\Delta_T \Delta_F = 1$, where Δ_T and Δ_F are distances between GFDM data symbols in time and frequency domain, respectively. Accordingly, the transmit signal $x^{(t)}[n]$ of one block of the tth transmit antenna equals

$$x^{(t)}[n] = \sum_{k \in \mathcal{K}} \sum_{m \mathcal{M}} g_{k,m}[n] d_{k,m}^{(t)}, \quad n = 0, \ldots, N-1 \tag{1}$$

$$g_{k,m}[n] = g[\langle n - mK \rangle_N] \exp(j2\pi \tfrac{kn}{K}), \tag{2}$$

where $\mathcal{K}$ and $\mathcal{M}$ denote the set of allocated subcarriers and subymbols, respectively. The prototype filter $g[n]$ is a band-limited filter such as a (root) raised cosine filter with rolloff α and hence, $\mathrm{DFT}_N\{g_{k,m}[n]\}[f] = 0, \forall |f - kM| > \frac{1+\alpha}{2} M$.

The linear modulation equation (1) is compactly written as

$$\vec{x}^{(t)} = \mathbf{A} \vec{d}^{(t)}, \tag{3}$$

where $\vec{x}^{(t)} = (x^{(t)}[n])_{n=0,\ldots,N-1}$ and $\mathbf{A}$ is a $N \times K_{\mathrm{on}} M_{\mathrm{on}}$ matrix, which contains all $(g_{k,m}[n])_{n=0,\ldots,N-1}$ as its columns. $K_{\mathrm{on}} \leq K$ and $M_{\mathrm{on}} \leq M$ are the cardinalities of $\mathcal{K}$ and $\mathcal{M}$, respectively. Further, $\vec{d}^{(t)}$ contains the transmitted data symbols $d_{k,m}^{(t)}$ in the appropriate order.

The signals propagate through independent Rayleigh block-fading multipath channels with channel impulse response (CIR) $h^{(r,t)}[n]$ between the tth transmit and rth receive antenna. By employing a cyclic prefix (CP) between subsequent GFDM blocks that is longer than the CIR, after CP removal at the receiver the convolution with the channel appears circular. Then, the received signal at the rth receive antenna equals

$$\vec{y}^{(r)} = \sum_{t=0}^{\bar{T}} \tilde{\mathbf{H}}^{(r,t)} \mathbf{A} \vec{d}^{(t)} + \vec{w}^{(r)}, \tag{4}$$

where $\tilde{\mathbf{H}}^{(r,t)}$ is the $N \times N$ circular convolution matrix based on the impulse response $h^{(r,t)}[n]$ and $\vec{w}^{(r)}$ denotes AWGN with distribution $\vec{w}^{(r)} \sim \mathcal{CN}(0, N_0 \mathbf{I})$.

Application of the N-point DFT matrix $\mathbf{F}$ to the signal received on each receiver antenna yields

$$\underbrace{\begin{pmatrix} \vec{Y}^{(0)} \\ \vdots \\ \vec{Y}^{\bar{R}} \end{pmatrix}}_{\vec{Y}} = \underbrace{\begin{pmatrix} \mathbf{H}^{(0,0)}\mathbf{F}\mathbf{A} & \ldots & \mathbf{H}^{(0,\bar{T})}\mathbf{F}\mathbf{A} \\ \vdots & \ddots & \vdots \\ \mathbf{H}^{(\bar{R},0)}\mathbf{F}\mathbf{A} & \ldots & \mathbf{H}^{(\bar{R},\bar{T})}\mathbf{F}\mathbf{A} \end{pmatrix}}_{\tilde{\mathbf{H}}} \underbrace{\begin{pmatrix} \vec{d}^{(0)} \\ \vdots \\ \vec{d}^{(\bar{T})} \end{pmatrix}}_{\vec{d}} + \vec{W}, \tag{5}$$

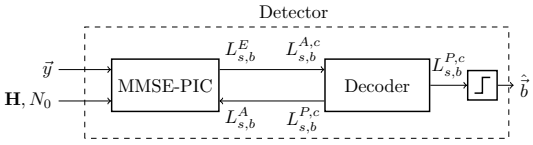

Fig. 2. Block diagram of iterative MIMO detection with using MMSE-PIC.

where $\mathbf{H}^{(r,t)} = \mathbf{F}\tilde{\mathbf{H}}^{(t,r)}\mathbf{F}^{\mathrm{H}}$ is a diagonal matrix containing $\mathbf{F}\vec{h}^{(t,r)}$ on the diagonal and $\vec{W}$ is the AWGN in the frequency domain. Accordingly, the columns in each block $\mathbf{H}^{(r,t)}\mathbf{FA}$ of $\tilde{\mathbf{H}}$ contain only $B = (1+\alpha)M$ non-zero elements. Now, consider a permutation matrix $\mathbf{P}$ such that $d^{(t)}_{k,m}$ appears at the $(t + Tm + TM_{\mathrm{on}}k)$th position of $\mathbf{P}\vec{d}'$ and let $\mathbf{H} = \tilde{\mathbf{H}}\mathbf{P}^{\mathrm{T}}$ be a column permutation of $\tilde{\mathbf{H}}$ so that

$$\vec{Y} = \mathbf{H}\vec{d} + \vec{W}, \tag{6}$$

where $\vec{d} = \mathbf{P}\vec{d}'$. Note that (6) models a general large-scale linear system, where readily available MIMO detection algorithms such as minimum mean square error (MMSE) or SD [10] detection can be applied in principle. In this paper, we analyze the performance of iterative MIMO detection for GFDM using a soft-in soft-out (SISO) MMSE-PIC demapper.

B. Iterative MMSE-PIC Detection

In the detector, soft information in terms of log-likelihood ratio (LLR) values is iteratively exchanged between the MMSE-PIC demapper and channel decoder, as shown in Fig. 2. The process starts with an initial MMSE guess of the transmitted bits by the MMSE-PIC demapper which is purely based on the received signal. The decoder refines this initial estimate and feeds back its a-posteriori information to the demapper. There, this information is used to pre-cancel interference before another MMSE demapping operation is performed. After several iterations, the final estimate of $\hat{\vec{b}}$ is given based on the signs of the a-posteriori LLR of the decoder. Note that compared to e.g. iterative turbo detection [18], instead of extrinsic information, we feed back a-posteriori information from the decoder to the demapper, such that the current estimate of the received signal is accurately cancelled from the received signal [19].

III. Parallel Interference Cancellation

A. Conventional MMSE-PIC Description

From the linear model (6), the SISO MMSE-PIC demapping algorithm as described in [20] is derived in the following. The process can be divided into 4 steps, given by

1) Computing soft-symbols from a-priori knowledge of the transmitted bits. The a-priori knowledge for the bth bit of the sth transmit symbol is encoded in the LLR value $L^A_{s,b}$ with $Pr[b_{s,b} = 1] = \frac{1}{1+\exp(L^A_{s,b})}$. Accordingly, the mean $\hat{d}_s$ and variance e_s of the estimate for the sth transmit symbol are

$$\hat{d}_s = \sum_{d\in\mathcal{S}} P[d_i = d]d \tag{7}$$

$$e_s = \sum_{d\in\mathcal{S}} P[d_s = d]\|d - \hat{d}_s\|^2. \tag{8}$$

2) Parallel interference cancellation. Let N_{on} and $\vec{h}_s$ denote the number of columns and the sth column of $\mathbf{H}$, respectively. For each symbol s, the estimated interference from all other symbols is cancelled from the received signal, leading to

$$\vec{Y}_s = \vec{Y} - \sum_{\substack{s'\neq s\\ s'=0}}^{N_{\mathrm{on}}-1} \vec{h}_{s'}\hat{d}_{s'} = \vec{h}_s d_s + \vec{n}, \tag{9}$$

where $\vec{n}$ is the remaining noise-plus-interference.

3) MMSE Filtering each signal $\vec{Y}_s$ with filter $\vec{w}^{\mathrm{H}}_s$. The filtering yields a new estimate $\hat{z}_s$ for the sth symbol, given by

$$\hat{z}_s = \vec{w}^{\mathrm{H}}_s\vec{Y}_s = \mu_s d_s + \vec{w}^{\mathrm{H}}_s\vec{n}, \tag{10}$$

where $\vec{w}^{\mathrm{H}}_s$ is the sth row of the matrix $\mathbf{W}^{\mathrm{H}}$ given by

$$\mathbf{W}^{\mathrm{H}} = \mathbf{X}^{-1}\mathbf{H}^{\mathrm{H}}, \tag{11}$$

with $\mathbf{X} = \mathbf{H}^{\mathrm{H}}\mathbf{H}\Lambda + N_0\mathbf{I}$, $\Lambda = \mathrm{diag}(e_1, \ldots, e_{N_{on}})$ and $\mu_s = \vec{w}^{\mathrm{H}}_s\vec{h}_s$. The remaining uncertainty $\mathrm{Var}[z_s]$ equals [20]

$$\mathrm{Var}[z_s] = \mu_s - e_s\mu_s^2. \tag{12}$$

4) Extrinsic LLR computation. From the refined soft-symbol estimates z_s, the LLRs $L^E_{s,b}$ are finally estimated by assuming that the noise terms $\vec{w}^{\mathrm{H}}_s\vec{n}$ on each z_s are independent and Gaussian distributed with variance $\mathrm{Var}[z_s]$. Application of the max-log approximation [24], the $L^E_{s,b}$ are approximated by

$$L^E_{s,b} = \frac{\mu_s^2}{\mu_s - e_s\mu_s^2}\left(\min_{d\in\mathcal{S}^{(0)}_b} |\tfrac{z_s}{\mu_s} - d|^2 - \min_{d\in\mathcal{S}^{(1)}_b} |\tfrac{z_s}{\mu_s} - d|^2\right), \tag{13}$$

where $\mathcal{S}^{(0)}_b, \mathcal{S}^{(1)}_b \subset \mathcal{S}$ are the subsets of all constellation symbols where the bth bit is 0 or 1, respectively [20].

B. Reduced Complexity Adaptation to GFDM

We propose a reformulation of the MMSE-PIC algorithm from [20] which can be implemented with significantly reduced complexity. It was already shown in [25] and [26] that steps 1) and 4) can be easily calculated, respectively. However, even though also the parallel interference cancellation (PIC) and MMSE filtering as formulated in [20] already offer reduced complexity compared to previously published approaches [27], [25], the algorithm and implementation in [20] proposes explicit calculation of $\mathbf{W}^{\mathrm{H}}$ by (11). Unfortunately, even in case $\mathbf{X}$ and $\mathbf{H}$ obey special structures such as some sparsity pattern to simplify the calculation of $\mathbf{W}^{\mathrm{H}}$, $\mathbf{W}^{\mathrm{H}}$ tends to be a fully occupied matrix. Hence, both storage of $\mathbf{W}^{\mathrm{H}}$ and explicit filtering via (10) can become prohibitively complex for large-scale systems. Instead, in this paper we

TABLE I
SUMMARY OF THE PROPOSED MMSE-PIC ALGORITHM, ASSUMING $\alpha = 1$, I.E. $B = 2M$.

	Calculation	Required multiplication count		Remark
Initialization	1) $\mathbf{G} = \mathbf{H}^{\mathrm{H}}\mathbf{H}$	$\frac{1}{2}2N_{\mathrm{on}}2M_{\mathrm{on}}T \cdot (BR)^2$	$= 8K_{\mathrm{on}}M_{\mathrm{on}}M^2R^2T$	(a)
	2) $Y_{\mathrm{MF}} = \mathbf{H}^{\mathrm{H}}\vec{Y}$	$N_{\mathrm{on}} \cdot BR$	$= 2K_{\mathrm{on}}M_{\mathrm{on}}MRT$	-
	3) $\mathbf{GV}$	$N_{\mathrm{on}}\mathcal{B} \cdot 2M_{\mathrm{on}}T$	$\approx 8K_{\mathrm{on}}M_{\mathrm{on}}^3T^3$	(b)
For each iteration	1) $\mathbf{X} = \mathbf{G}\Lambda + \sigma_n^2\mathbf{I}$	$N_{\mathrm{on}} \cdot 4M_{\mathrm{on}}T$	$= 4K_{\mathrm{on}}M_{\mathrm{on}}^2T^2$	-
	2) $\mathbf{X} = \mathbf{LU}$	$2N_{\mathrm{on}} \cdot 2M_{\mathrm{on}}T(3M_{\mathrm{on}}T + 1)$	$\approx 12K_{\mathrm{on}}M_{\mathrm{on}}^3T^3$	(c)
	3) $\vec{n}_0 = Y_{\mathrm{MF}} - \mathbf{G}\vec{d}$	$N_{\mathrm{on}} \cdot 4M_{\mathrm{on}}T$	$= 4K_{\mathrm{on}}M_{\mathrm{on}}^2T^2$	-
	4) $\vec{u} = (\mathbf{LU})^{-1}\vec{n}_0$	$2N_{\mathrm{on}} \cdot 6M_{\mathrm{on}}T$	$= 12K_{\mathrm{on}}M_{\mathrm{on}}^2T^2$	(d)
	5) $\mathcal{X} = \mathbf{X}^{-1}(\mathbf{GV})$	$2N_{\mathrm{on}} \cdot 6M_{\mathrm{on}}T \cdot \mathcal{B}$	$\approx 48K_{\mathrm{on}}M_{\mathrm{on}}^3T^3$	(b),(d)
	6) $\vec{\tilde{\mu}} = [(\mathbf{V} \circ \mathcal{X})\vec{1}] \oslash [(\mathbf{V} \circ \mathbf{V})\vec{1}]$	$N_{\mathrm{on}}\mathcal{B}$	$\approx 2K_{\mathrm{on}}M_{\mathrm{on}}^2T^2$	(b),(e)

(a) $\frac{1}{2}$ arises from the fact that $\mathbf{G}$ is Hermitian and hence the lower triangular part can be inferred from the upper part.
(b) Assuming $\mathcal{B} = 4M_{\mathrm{on}}T$
(c) Operation count taken from [23, Function *zgbtrf*]
(d) Operation count taken from [23, Function *zgbtrs*]
(e) Only $\mathbf{V} \circ \mathcal{X}$ counts, as $(\mathbf{V} \circ \mathbf{V})\vec{1} = \lceil 4M_{\mathrm{on}}T \rceil_2 \vec{1}$ and division is implemented by simple bitshift.

propose an algorithm that can exploit special structure of a given $\mathbf{H}$ for an implementation with reduced complexity.

We start by reformulating (9) to

$$\vec{Y}_s = \vec{Y} - \mathbf{H}\vec{\hat{d}} + \vec{h}_s\hat{d}_s \tag{14}$$

where $\vec{\hat{d}}$ is the vector of all soft-symbol estimates from (7). Now, from (10) we have

$$\vec{\tilde{z}} = \mathbf{X}^{-1}(\vec{Y}_{MF} - \mathbf{G}\vec{\hat{d}}) + \mathrm{diag}(\mathbf{X}^{-1}\mathbf{G}) \circ \vec{\hat{d}}, \tag{15}$$

where $\vec{Y}_{\mathrm{MF}} = \mathbf{H}^{\mathrm{H}}\vec{Y}$ and $\mathbf{G} = \mathbf{H}^{\mathrm{H}}\mathbf{H}$ is the Gram matrix of the columns of $\mathbf{H}$. Hence, instead of explicitely calculating $\mathbf{W}^{\mathrm{H}}$ to calculate the PIC and MMSE filtering in (15), it suffices to know the solution of

$$\vec{u} = \mathbf{X}^{-1}(\vec{Y}_{\mathrm{MF}} - \mathbf{G}\vec{\hat{d}}) \tag{16}$$

and

$$\vec{\mu} = \mathrm{diag}(\mathbf{X}^{-1}\mathbf{G}). \tag{17}$$

For GFDM, each column of $\mathbf{H}$ contains only BR non-zero elements, hence ICI only appears between adjacent subcarriers. Accordingly, $\mathbf{G} = \mathbf{H}^{\mathrm{H}}\mathbf{H}$ becomes a band-diagonal matrix with upper and lower bandwidth $2M_{\mathrm{on}}T$. Then, LU decomposition of $\mathbf{X}$ and forward-backward substitution is performed with complexity that scales linear with matrix size and quadratic with bandwidth [23, Functions *zgbtrf, zgbtrs*].

In order to calcuate $\vec{\mu}$, we can resort to an estimation procedure as shown in [22]. Instead of explicitely calculating $\mathbf{X}^{-1}\mathbf{G}$, we calculate $\mathcal{X} = \mathbf{X}^{-1}(\mathbf{GV})$ where $\mathbf{V}$ is an arbitrary real matrix. Then, an estimate of $\vec{\mu}$ is given by

$$\vec{\tilde{\mu}} = [(\mathbf{V} \circ \mathcal{X})\vec{1}] \oslash [(\mathbf{V} \circ \mathbf{V})\vec{1}]. \tag{18}$$

The accuracy of the estimation depends on both the structure of $\mathbf{V}$ and $\mathbf{X}^{-1}\mathbf{G}$. In general, the estimation (18) is exact, if the off-diagonal elements of $\mathbf{VV}^{\mathrm{T}}$ are zero where $\mathbf{X}^{-1}\mathbf{G}$ is non-zero. Optimally, $\mathbf{V} = \mathbf{I}$, however in this case the inverse is implicitely calculated, leading to no reduction in complexity.

Instead, noting that both $\mathbf{X}$ and $\mathbf{G}$ are band-diagonal, we can assume that $\mathbf{X}^{-1}\mathbf{G}$ is mostly concentrated within the bandwidth $4M_{\mathrm{on}}T$. We then design a $\mathbf{V}$ such that $\mathbf{VV}^{\mathrm{T}}$ is zero within the bandwidth $4M_{\mathrm{on}}T$. A straight forward approach are submatrices of Hadamard matrices, as shown in [22]. Let $\mathcal{H}$ denote the Hadamard matrix of dimension $\lceil N_{\mathrm{on}} \rceil_2$. Then, $\mathbf{V}$ is given as the first N_{on} rows and first $\mathcal{B} = \lceil 4M_{\mathrm{on}}T \rceil_2$ columns of $\mathcal{H}^{\mathrm{T}}$. With this operation, we obtain a matrix $\mathbf{V}$ where $\mathbf{VV}^{\mathrm{T}}$ is zero within the bandwith $4M_{\mathrm{on}}T$ [22] and accordingly, (18) yields accurate results. By estimating the diagonal in (17), the number of right-hand-sides in (17) is only proportional to the bandwidth $\mathbf{X}$ instead of its overall size. Hence, the complexity does not depend on the number of allocated subcarriers, keeping overall complexity low.

The proposed algorithm for PIC and MMSE filtering is summarized in Tab. I, where also the number of required complex multiplications for each step is listed. Note that the overall complexity is linear with the number of allocated subcarriers and cubic with the number of allocated subsymbols and transmit antennas. This result is reasonable, since $M_{\mathrm{on}}T$ symbols overlap on each received frequency bin, and accordingly, we expect a cubic complexity for the corresponding matrix inversion. On the other hand, since the number of interfering symbols does not depend on the number of subcarriers, there exists an algorithm that scales linearly with the number of subcarriers K_{on}. For comparison, performing the proposal from [20] for the detection, we end up with a complexity that scales quadratically with the number of subcarriers and cubic with the number of subsymbols and transmit antennas, when already taking advantage of the fact that $\mathbf{G}$ is band diagonal.

Note that the proposed algorithm can also be suitable for massive MIMO systems, where the Gram matrix $\mathbf{G}$ tends to be diagonally dominant [28] and equally, efficient solutions to (16) and (17) can be found.

IV. NUMERICAL RESULTS

A. Information Transfer Characteristic

As a performance metric that is independent of the chosen channel channel code, the information transfer charts of the MMSE-PIC demapper for GFDM and OFDM with different

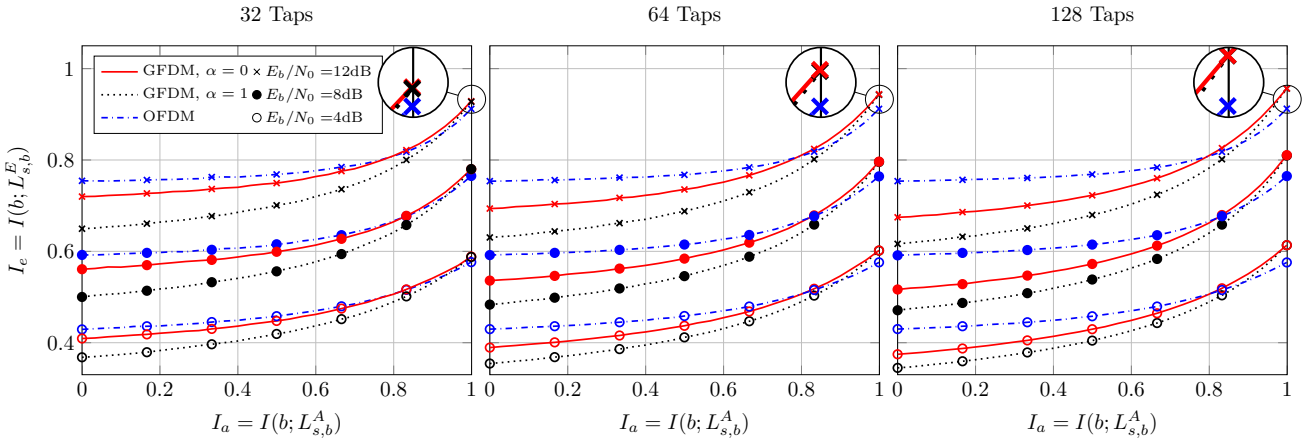

Fig. 3. Information transfer chart for the MMSE-PIC demapper. E_b/N_0 denotes receive SNR.

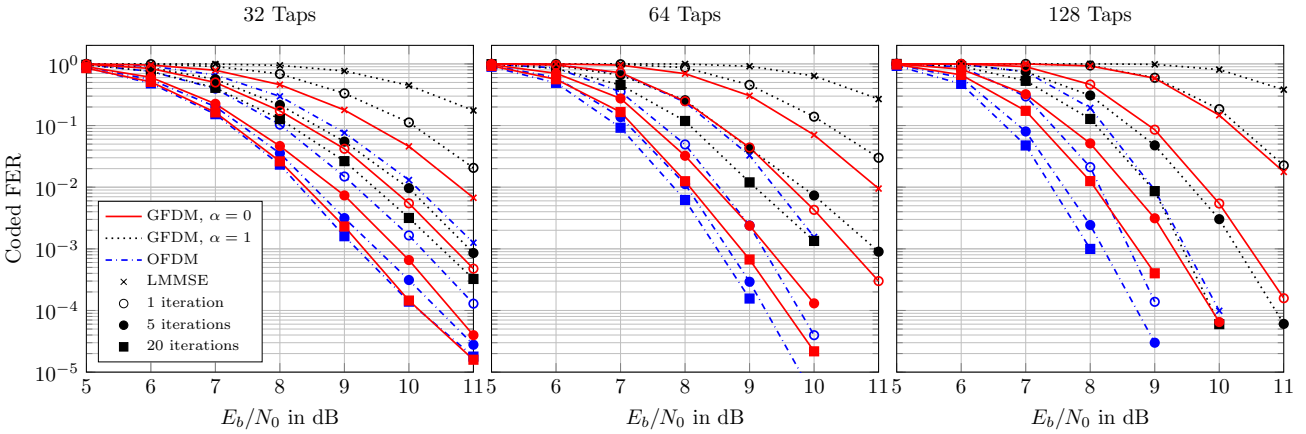

Fig. 4. Coded FER for different channel lengths. LMMSE means no feedback iteration has been performed.

TABLE II
SIMULATION PARAMETERS

Parameter	Symbol	GFDM	OFDM
# Available Subcarriers	K	64	$7 \cdot 64$
# Allocated Subcarriers	K_{on}	48	$7 \cdot 48$
# Subsymbols	M	7	1
# Allocated Subsymbols	M_{on}	7	1
# Number of Tx, Rx antennas	T, R	2	2
Prototype filter	$g[n]$	raised cosine (RC)	Rect
Filter rolloff	α	0 or 1	-
Modulation order	$\mathcal{S}$	64-QAM	
Channel Model		Uniform PDP, 32, 64 or 128 taps	
Code	-	WiMax LDPC block code	
Code rate	-	$1/2$	
Code block length	-	2016 bits	

rolloffs and channel lengths, using the system parameters from Tab. II are shown in Fig. 3 where a contiguous subcarrier allocation is considered. It is assumed that the transmitter and receiver are ideally synchronized and perfect CSI is available at the receiver. In the simulation, independent block Rayleigh-fading channels with uniform power delay profile (PDP) are assumed. The a-priori LLR $L^A_{s,b}$ are generated as independend Gaussian random variables with distribution $L^A_{s,b} \sim \mathcal{N}(\pm\frac{\sigma_A^2}{2}, \sigma_A^2)$, where σ_A^2 is calculated from the inverse J-function $\sigma_A^2 = J^{-1}(I(b; L^A_{s,b}))$ [24]. At the output of the demapper, the mutual information $I(b; L^E_{s,b})$ between b and $L^E_{s,b}$ is measured with the histogram approach from [29].

As can be seen, for the initial iteration (i.e. $I_a = 0$), the OFDM system outputs higher extrinsic information than the GFDM system. The gap to the OFDM system increases with the channel length, rolloff and SNR. This observation can be explained by the amount of interference that occurs in the system. For the OFDM system, only inter-antenna interference (IAI) occurs, whereas for GFDM with $\alpha = 0$ IAI and ISI appears. Finally, with $\alpha = 1$, 3-dimensional interference IAI, ISI and ICI occurs which needs to be cancelled by the system.

Initially, the MMSE demapper performs worse, with more interference. When the a-priori information in the system increases, the extrinsic information I_e of the the GFDM systems approaches that of OFDM and at approximately $I_a = 0.8$, GFDM outperforms OFDM. For perfect a-priori information, i.e. $I_a = 1$, GFDM achieves a higher I_e than OFDM. The gap

increases with the channel length. This suggests the possibility that GFDM with a well-designed code can indeed outperform OFDM in severely frequency selective channels, as has been forecast in [17] and was also numerically proved in [14].

B. Simulation of Frame Error Rate

Fig. 4 compares the coded FER of a GFDM and an OFDM system using the MMSE-PIC iterative receiver structure for different channel lengths. The channel code counterpart was chosen to be a state-of-the-art WiMax half-rate low-density parity check (LDPC) block code due to its reduced latency and implementation complexity compared to Turbo codes [30], [31], [32]. As visible, performing iterative detection can significantly reduce the FER.

For OFDM, the gain between no iterations and the converged system at 20 iterations equals $1.8, 1.6$ and 1.6dB at a FER of 10^{-2} for 32, 64 and 128 channel taps, respectively. For the GFDM system with $\alpha = 0$, the gain increases with the channel length from 2.4dB to 3.2dB for 32 and 128 taps, respectively. The GFDM system with full rolloff $\alpha = 1$ exhibits very poor performance compared to the OFDM system. On the other hand, this system benefits most from the iterative detection process, as the gain is several dB for a FER of 10^{-2} and increases with the channel length.

This behaviour can be explained with the information transfer chart in Fig. 3. At the initial iteration, the higher the interference, the lower the output mutual information and hence the higher the FER. By performing iterations between decoder and demapper, the a-priori knowledge in the system increases, and due to the steeper slope of systems with higher interference, more gain is achieved with iterative detection.

Nethertheless, with the presented combination of the decoder, the OFDM system outperforms both GFDM systems. The gap between OFDM and GFDM with $\alpha = 0$ increases with the channel length, being marginal for 32 taps, but increasing to 0.6dB for a channel length of two subsymbols. This suggests that the choice of the code and decoding algorithm is not optimal for the present system, since the potential of the GFDM system is not fully utilized. Instead, the higher extrinsic information output of the OFDM demapper at lower I_a explains the observed behaviour. This observation implies that the employed channel code and decoding algorithm should be carefully designed jointly with the waveform, in order to exploit the full potential of the GFDM system. The design of such an optimized code is out of scope of this paper and devoted to future work.

C. Influence of Imperfect Estimation of $\vec{\mu}$

Considering Tab. I, the estimation of the mean $\vec{\mu}$ is the most expensive part of the demapping algorithm. Hence it is beneficial to analyze the influence of the number of columns of $\mathbf{V}$ on the accuracy of the estimation. Tab. III shows the according results, where the values are $10\log_{10}\Delta_\mu^2$ with

$$\Delta_\mu^2 = \frac{(\vec{\mu}-\hat{\vec{\mu}})^{\mathrm{H}}(\vec{\mu}-\hat{\vec{\mu}})}{\vec{\mu}^{\mathrm{H}}\vec{\mu}}, \tag{19}$$

TABLE III
DEVIATION OF THE ESTIMATED FROM THE EXACT MEAN IN RELATION TO THE NUMBER OF COLUMNS $\mathcal{B}$ IN (18). THE VALUES ARE GIVEN IN dB.

$\mathcal{B} = \frac{\lceil 4M_{\mathrm{on}}T\rceil_2}{x}$	$x =$	$\frac{1}{2}$	1	2	4	8
RC with $\alpha = 0$	$\Delta_\mu^2 =$	$-\infty$	$-\infty$	$-\infty$	-45	-32
RC with $\alpha = 1$	$\Delta_\mu^2 =$	-85	-48	-21	-19	-12

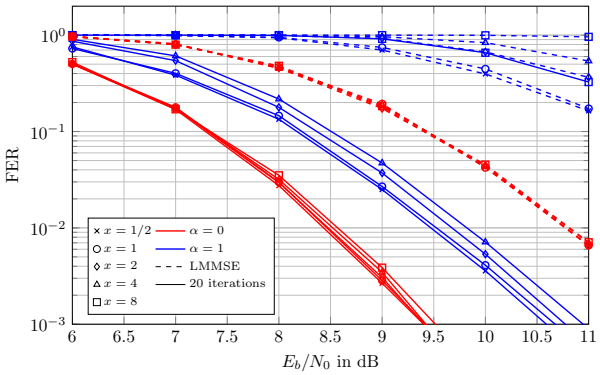

Fig. 5. Simulated FER for different number $\mathcal{B}$ of columns of $\mathbf{V}$ in (18). x matches the value in Tab. III.

where $\hat{\vec{\mu}}$ and $\vec{\mu}$ are from (18) and (17), respectively.

As shown, for $\alpha = 0$, the estimation is exact for column counts of $\mathbf{V}$ above $\lceil M_{\mathrm{on}}T\rceil_2$ and only small deviations appear for even smaller column counts. This can be explained that in case of $\alpha = 0$, $\mathbf{G}$ is essentially a block-diagonal matrix with no ICI. Accordingly $\mathbf{X}^{-1}$ is also block-diagonal with the same bandwidth. Hence, as long as the column count of $\mathbf{V}$ is above this bandwidth, the estimation is accurate. For $\alpha = 1$, $\mathcal{B}$ has more influence on the estimation accuracy, ranging from -80dB for a large column count up to -12dB deviation for $\mathcal{B} = \frac{1}{2}\lceil M_{\mathrm{on}}T\rceil_2$. This behaviour is caused by the truly band-diagonal structure of $\mathbf{G}$, and hence $\mathbf{X}^{-1}$ is only approximately band-diagonal. Hence, estimating $\vec{\mu}$ is not exact and the more columns in $\mathbf{V}$ are used, the more accurate is the estimation.

Fig. 5 illustrates the effect of imperfect estimation of $\vec{\mu}$ on the achieved FER of the GFDM system. As shown for $\alpha = 0$, only for $x = 8$ a slight degradation is visible for the converged system with 20 iterations. No difference can be seen for the pure LMMSE detection without feedback from the decoder. This suggests, that the number of columns of $\mathbf{V}$ can be reduced even further without degrading the demapping performance. On the other hand for $\alpha = 1$, $\mathcal{B}$ has a stronger influence on the system performance. In particular, there is a vast gap between $x = 4$ and $x = 8$, showing that an estimation error of $\Delta_\mu^2 = -12$dB is not tolerable by the system. However, for larger $\mathcal{B}$, the performance degradation in particular after 20 iterations is only 0.25dB away from the accurate estimation of $\vec{\mu}$. Again, this observation reveals, that the number of columns of $\mathbf{V}$ can be further reduced to save complexity.

V. Conclusion

This paper applies the MMSE-PIC demapping algorithm to an iterative receiver structure for GFDM. Compared to direct application of the algorithm from [20], by exploiting the band-diagonal structure of the system, we provide a significantly reduced complexity formulation of the demapping process which scales linearly with the number of subcarriers in the system. Additionally, applying an algorithm for the estimation of the diagonal of a matrix without explicitely calculating this matrix reduces complexity even further, where have presented the tradeoff between estimation accuracy and algorithm complexity. Using the standard WiMax LDPC codes, GFDM performs worse than OFDM. However, the analysis of the information transfer characteristics of the MMSE-PIC demapper for GFDM suggests, that a superior performance compared to OFDM can be achieved in rich multipath environments, given that the channel decoding counterpart is suitably designed. This observation motivates the design of such a suitable code, which is an open topic and devoted to future research.

VI. Acknowledgements

The work presented in this paper was sponsored by the Federal Ministry of Education and Research within the programme "Twenty20 - Partnership for Innovation" under contract 03ZZ0505B - "fast wireless". The computations were performed at the Center for Information Services and High Performance Computing (ZIH) at TU Dresden.

References

[1] G. Wunder, P. Jung, M. Kasparick, T. Wild, F. Schaich, Y. Chen, S. Brink, I. Gaspar, N. Michailow, A. Festag, L. Mendes, N. Cassiau, D. Ktenas, M. Dryjanski, S. Pietrzyk, B. Eged, P. Vago, and F. Wiedmann, "5GNOW: non-orthogonal, asynchronous waveforms for future mobile applications," *IEEE Communications Magazine*, vol. 52, no. 2, pp. 97–105, feb 2014.

[2] Q. Sun, C.-L. I, S. Han, Z. Xu, and Z. Pan, "Software defined air interface: a framework of 5G air interface," *2015 IEEE Wireless Communications and Networking Conference Workshops (WCNCW)*, pp. 6–11, 2015.

[3] Y. Chen, F. Schaich, and T. Wild, "Multiple Access and Waveforms for 5G: IDMA and Universal Filtered Multi-Carrier," in *2014 IEEE 79th Vehicular Technology Conference (VTC Spring)*. IEEE, may 2014, pp. 1–5.

[4] M. Bellanger, "FBMC physical layer: a primer," PHYDYAS, Tech. Rep., 2010.

[5] N. Michailow, M. Matthé, I. Gaspar, A. Navarro Caldevilla, L. L. Mendes, A. Festag, and G. Fettweis, "Generalized Frequency Division Multiplexing for 5th Generation Cellular Networks," *IEEE Transactions on Communications*, vol. 62, no. 9, pp. 3045–3061, 2014.

[6] M. Matthé, L. L. Mendes, and G. P. Fettweis, "Asynchronous Multi-User Uplink Transmission with Generalized Frequency Division Multiplexing," in *International Workshop on Advanced PHY and MAC Techniques for Super Dense Wireless Networks (IWSDN) in Conjunction with ICC*, 2015.

[7] A. Farhang, N. Marchetti, and L. E. Doyle, "Low Complexity Modem Design for GFDM," *IEEE Transactions on Signal Processing*, vol. PP, no. 99, pp. 1–1, 2015.

[8] Y. Rui, P. Cheng, M. Li, Q. T. Zhang, and M. Guizani, "Carrier aggregation for LTE-advanced: Uplink multiple access and transmission enhancement features," *IEEE Wireless Communications*, vol. 20, no. 4, pp. 101–108, 2013.

[9] T. S. Rappaport, S. Sun, R. Mayzus, H. Zhao, Y. Azar, K. Wang, G. N. Wong, J. K. Schulz, M. Samimi, and F. Gutierrez, "Millimeter wave mobile communications for 5G cellular: It will work!" *IEEE Access*, vol. 1, pp. 335–349, 2013.

[10] S. Yang and L. Hanzo, "Fifty Years of MIMO Detection: The Road to Large-Scale MIMOs," *IEEE Communications Surveys & Tutorials*, vol. 17, no. 4, pp. 1941–1988, 2015.

[11] L. Lu, S. Member, G. Y. Li, and A. L. Swindlehurst, "An Overview of Massive MIMO : Bene fi ts and Challenges," *Ieee Journal of Selected Topics in Signal Processing*, vol. 8, no. 5, pp. 742–758, 2014.

[12] M. Matthé, L. Mendes, N. Michailow, D. Zhang, and G. Fettweis, "Widely Linear Estimation for Space-Time-Coded GFDM in Low-Latency Applications," *IEEE Transactions on Communications*, vol. 63, no. 11, pp. 4501–4509, 2015.

[13] M. Matthe, L. L. Mendes, I. Gaspar, N. Michailow, D. Zhang, and G. Fettweis, "Multi-user time-reversal STC-GFDMA for future wireless networks," *EURASIP Journal on Wireless Communications and Networking*, vol. 2015, no. 1, p. 132, may 2015.

[14] D. Zhang, L. Mendes, M. Matthe, I. Gaspar, N. Michailow, and G. Fettweis, "Expectation Propagation for Near-Optimum Detection of MIMO-GFDM Signals," *IEEE Transactions on Wireless Communications*, vol. 15, no. 2, pp. 1045 – 1062, 2015.

[15] M. Matthé, I. Gaspar, D. Zhang, and G. Fettweis, "Short Paper: Near-ML Detection for MIMO-GFDM," in *Proceedings IEEE 82nd Vehicular Technology Conference*, Boston, 2015.

[16] N. E. Tunali, M. Wu, C. Dick, C. Studer, and S. Jose, "Linear Large-Scale MIMO Data Detection for 5G Multi-Carrier Waveform Candidates," in *Asilomar Conference on Signals, Systems, and Computers*, 2015, pp. 1–5.

[17] D. Zhang, Matthé, Maximilian, L. L. Mendes, and G. Fettweis, "Message Passing Algorithms for Upper and Lower Bounding the Coded Modulation Capacity in a Large-scale Linear System," *IEEE Signal Processing Letters*, vol. Accepted f, 2015.

[18] X. Wang and H. Vincent Poor, "Iterative (Turbo) soft interference cancellation and decoding for coded CDMA," *IEEE Transactions on Communications*, vol. 47, no. 7, pp. 1046–1061, 1999.

[19] M. Witzke, S. Baro, F. Schreckenbach, and J. Hagenauer, "Iterative detection of MIMO signals with linear detectors," *Conference Record of the Thirty-Sixth Asilomar Conference on Signals, Systems and Computers, 2002.*, vol. 1, pp. 0–4, 2002.

[20] C. Studer, S. Fateh, and D. Seethaler, "ASIC implementation of soft-input soft-output MIMO detection using MMSE parallel interference cancellation," *IEEE Journal of Solid-State Circuits*, vol. 46, no. 7, pp. 1754–1765, 2011.

[21] J. Liu, S. Liu, Z. Luo, and Y. Liu, "MMSE-PIC MUD for CDMA-Based MIMO-OFDM System," in *Proceedings of ISCIT2005*, 2005, pp. 510–513.

[22] C. Bekas, E. Kokiopoulou, and Y. Saad, "An estimator for the diagonal of a matrix," *Applied Numerical Mathematics*, vol. 57, no. 11-12, pp. 1214–1229, 2007.

[23] T. N. A. G. (NAG), "The NAG Library," Oxford, UK.

[24] W. Ryan and S. Lin, *Channel Codes: Classical and Modern*, 2009.

[25] A. Tomasoni, M. Ferrari, D. Gattit, F. Osnatot, and S. Bellini, "A low complexity turbo MMSE receiver for W-LAN MIMO systems," *IEEE International Conference on Communications*, vol. 9, no. c, pp. 4119–4124, 2006.

[26] S. Häne, "VLSI circuits for MIMO-OFDM physical layer," Ph.D. Dissertation, ETH Zürich, Switzerland, 2008.

[27] M. Tüchler, A. C. Singer, and R. Koetter, "Minimum mean squared error equalization using a priori information," *IEEE Transactions on Signal Processing*, vol. 50, no. 3, pp. 673–683, 2002.

[28] P. J. Smith, C. Neil, M. Shafi, and P. a. Dmochowski, "On the convergence of massive MIMO systems," *Communications (ICC), 2014 IEEE International Conference on*, pp. 5191–5196, 2014.

[29] P. Fertl, J. Jaldén, and G. Matz, "Performance assessment of MIMO-BICM demodulators based on mutual information," *IEEE Transactions on Signal Processing*, vol. 60, no. 3, pp. 1366–1382, 2012.

[30] K. K. Gunnam, G. S. Choi, M. B. Yeary, and M. Atiquzzaman, "VLSI architectures for layered decoding for irregular LDPC codes of WiMax," *IEEE International Conference on Communications*, pp. 4542–4547, 2007.

[31] M. Landolsi, "A Comparative Performance and Complexity Study of Short-Length LDPC and Turbo Product Codes," in *2006 2nd International Conference on Information & Communication Technologies*, vol. 2. IEEE, 2006, pp. 2359–2364.

[32] TurboBest, "IEEE 802.16e LDPC Encoder/Decoder Core," Tech. Rep., 2006.